ARTICLE TEMPLATE

Characterising Nematic Liquid Crystals Using a Circular Patch Resonator

Qiang Wu[a], Yongwei Zhang[a], Haofeng Peng[a] and Murat Temiz[b]

[a]School of Transportation, Nantong University, Nantong, Jiangsu Province, 226019, China
[b]Department of Electronic and Electrical Engineering, University College London, London, WC1E 7JE, UK

ARTICLE HISTORY
Compiled June 1, 2023

ABSTRACT
Reconfigurable microwave material is a promising candidate for designing and manufacturing tunable microwave components. Nematic liquid crystals (NLC) are such materials since their permittivity can be tuned by an external electric field. However, many NLC mixtures were not properly characterized at higher frequency bands due to requiring a complex measurement setup. In this work, a novel method using circular patch resonator (CPR) is developed to measure the dielectric constant and loss tangent of NLCs at microwave frequencies. In addition to using the cavity model for the preliminary design and analyzing the fringing effect for a better accuracy, full-wave simulations are employed to confirm the final design and aid the characteristic analysis. Three prototypes were fabricated and measured to reduce uncertainty from manufacturing defects. To avoid the possible damage when higher voltage is required for a large range tuning, a coupling mechanism is proposed between the microstrip line and coplanar waveguides (CPWs) to replace connection through vias. A high accuracy with an uncertainty of 0.02 for relative permittivity estimate has been demonstrated with experiment verification, approximate 80% improvement than other typical methods. The simple design and PCB-based manufacturing techniques can be widely employed to characterize the properties of newly-developed LC mixtures.

KEYWORDS
Cavity model; dielectric measurements; full-wave analysis; millimeter-wave devices; nematic liquid crystal

1. Introduction

Microwave-based technologies play an important role in today's society, which utilize frequencies in the millimeter-wave (mmWave) regime so as to obtain the necessary large bandwidth and satisfy the demand of higher data rates. In some communication systems, such as 5G and low-orbit satellite systems, ground mobile terminals might access the communication infrastructure via beam-steering antenna arrays to increase the coverage and reduce the latency [1,2]. To implement such devices with the function of beam steering, different methods employing various materials and techniques have been used, such as semiconductor [3], RF Micro-electromechanical systems (MEMS) [4], ferroelectrics [5] and liquid crystals (LCs) [6]. However, for systems with a large

CONTACT Yongwei Zhang. Email: david.y.zhang@ntu.edu.cn

number of beams, it is not practical to be steered by the bulky mechanical systems when the ground terminals are moving. Hence, smart RF components with compact and low insertion loss properties are demanded to adjust the beams for more efficient use of spectrum resources. To design and manufacture such smart RF components, LC shows a promising characteristic. Based on their unique birefringence property, LC materials are initially utilized mainly for the optical applications (e.g., displays, lenses, etc.) [7,8]. In the last two decades, following the evolution of microwave techniques, novel nematic liquid crystal (NLC) has drawn significant attention because of its large anisotropy and low loss characteristic at higher frequency band. In addition, compared to the conventional ferroelectric materials, the main advantages of LC material are lower voltages required for tunability and being moderately low cost. Therefore, NLCs are promising materials for reconfigurable millimeter-wave applications [9,10]. Several types of applications based on NLC have been demonstrated in the literature, such as phase shifters [11–13], tunable reflectarray antennas [14], dielectric waveguides [15,16], and steerable phased arrays [17–19].

Some studies have been carried out to determine the properties of LC materials in the literature. Early study for characterising the properties was presented in the 1950s, which applying a magnetic field to align the orientation of LC for a fast proof-of-concept in the lab [20]. Nowadays, with the development of microwave devices, several technologies covering a large frequency range have been proposed to estimate the characteristics of LCs with help of an electric biasing, which can be classified as a broadband method and resonator-based method. Broadband methods can determine the dielectric properties over a broad frequency range while the measurements of permittivity usually are not accurate enough. Thus, they are very useful for applications in higher frequency bands (e.g., above 30 GHz for optical components). Some methods, such as temperature-controlled coaxial transmission line [21] and a covered microstrip line [22,23], have been proposed to obtain a rough estimate of LC properties.

Compared with the broadband methods, resonator-based techniques can estimate the parameters with a higher accuracy but only at single or some discrete frequencies, and are primarily applied in low microwave frequency range. Meanwhile, one of advantages is that the resonate frequencies and other properties can be accurately analyzed by means of a cavity model. Several methods such as using a split-cylinder ring [24,25], a patch resonator [26], a circular patch resonator (CPR) [27], and an inductive coupled ring resonator [28], have been reported in the literature. In [24], it can yield ± 0.22 uncertainty on permittivity measurement for QYPD-036 material by using a split-cylinder ring. In contrast to a microstrip line resonator [22], a CPR with a cavity can tune a larger volume of LC, which potentially leading to a better orientation alignment of the molecules, accordingly a better accuracy is expected. In [27], a CPR was also used to determine the permittivity but a complex experimental setup is needed. In addition, compared with [27], this work provided a numerical approximation that allows a better prediction of the effective circular radius, and achieves a higher accuracy for dielectric constant determination.

In this work, a low-cost printed circuit board (PCB)-based CPR with high resolution is designed, fabricated, and tested to determine the dielectric constant and loss tangent of the newly developed off-the-shelf NLCs. An cavity model is developed to investigate the relationship between the physical dimension and resonant frequency of the CPR. The parameters of the cavity model are verified by a full-wave simulator. Finally, one CPR is designed and three samples are fabricated and measured. The experimental results from vector network analyzer (VNA) had a good agreement with those from the full-wave simulation, as well as the cavity model. It should be noted

that the proposed CPR has an operating frequency lower than 10 GHz based on the following considerations: i) there are many wireless applications operating in sub-10 GHz frequencies including 5G and low-orbit satellite communication system; ii) the manufacturing cost is relatively low, meanwhile it is easier to analyze the measurement uncertainty; iii) permittivity ε keeps reasonably constant over this frequency range, while it has relatively large variation in other higher millimetre wave frequency bands.

The main contributions of this investigation are as follows:

- The proposed design is solely based on a PCB technology without involving a complex process as in the existing methods, hence it is applicable in most scenarios where accurate characterisation are required for high-tunability devices at a low cost.
- Compared to other methods such as in [27], this study considers the fringing effect of circular patch, therefore yields a better accuracy. The error of the permittivity in the proposed method is less than 0.02, which was typically over 0.1 based on the previous methods.
- To calculate ε_r with respect to the resonant frequency, a closed-form expression has been derived to determine the effective radius a_e by decoupling the permittivity ε_r where a_e and ε_r have a high correlation.
- To avoid possible damage to the instrument caused by external high bias voltages required for a large range of tuning, this study utilizes a coupling mechanism, which is beneficial for applications that require a higher bias voltage as it is isolated for DC between the microstrip line and two CPWs for feed.

The paper is organised as follows: Section 2 introduces the cavity model of a CPR and presents a closed-form expression with respect to the resonant frequency and the permittivity of the LC material; Section 3 first describes the design and fabrication of the CPR, then the experimental results and the uncertainty analysis are provided, finally the uncertainty of the proposed CPR are compared to those by other typical methods in the literature; The conclusion is presented in Section 4.

2. Material and methods

As an anisotropic material, the unique feature of nematic LC is that the direction of LC molecules can be re-oriented, by means of an external low-frequency electric or magnetic field, which can then lead to different dielectric constants. Anisotropy is the key characteristic attractive in microwave devices. According to the orientation of LC molecules, the permittivity of LC can be simply represented as a tensor vector from the parallel direction $\varepsilon_{\parallel}$ to the perpendicular direction $\varepsilon_{\perp}$, as shown in Figure 1. Anisotropy can be defined as the maximal difference of these two extreme values, $\Delta\varepsilon = \varepsilon_{\parallel} - \varepsilon_{\perp}$.

The choice of LC material for a microwave device depends on some intrinsic parameters, such as permittivity, loss tangent and Frank elastic constants, etc. Among these parameters, elastic constants are mainly considered in optical applications, and out of scope of this work. Loss tangent is a useful parameter to evaluate the dissipation factor of RF devices, and can be derived from the quality factor. Both the relative permittivity and loss tangent have been examined in this study due to their importance for the design of microwave components.

Taking conventional phase shifter as an example, the maximal phase delay $\Delta\Phi$ mainly depends on the physical length of shifter l and two extreme dielectric constants

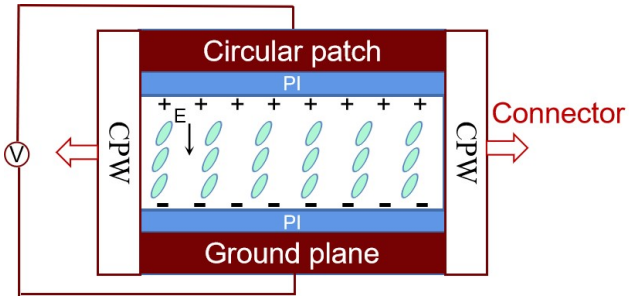

Figure 1. Orientation of LC molecules under different biasing voltages.

$\varepsilon_{\parallel}$ and $\varepsilon_{\perp}$, can be written as [13]:

$$\Delta\Phi = \frac{2\pi l f}{c}(\sqrt{\varepsilon_{\parallel}} - \sqrt{\varepsilon_{\perp}}) \tag{1}$$

where f is the operating frequency, c is the speed of light.

Several LC mixtures initially designed for the display devices, such as E7 (Merck KGaA), K15 (5CB), etc., have been used for the microwave components. However, they demonstrate relatively small anisotropy and high loss tangent at mmW frequency band. Recently some high performance LC materials have been developed to meet the demand of microwave applications, e.g., GT7-29001 provided by Merck KGaK showing a large anisotropy ($\Delta\varepsilon_r > 1$ at 19 GHz), but it is not widely available. In addition, some LC mixtures might have a great potential for the microwave applications, but they only provide parameters for the optical devices, and their characteristics at the microwave frequency band need to be thoroughly examined. Thus, to achieve the optimal performance of LC-based microwave devices, it is very important to develop low-cost and easily implemented technique to accurately determine the characterization of various LC materials.

This study uses a CPR to analyze the characteristics of LC because of its simple structure and high estimation accuracy. A basic model of CPR is shown in Figure 2. In contrast to examining structures with a rectangular patch and transmission line, we used the cylindrical coordinate (ρ, ϕ, z) system to investigate CPRs. In addition, only one parameter (radius a of the disc) is needed to determine the orders of electromagnetic modes. For LC-based CPR design, the circular patch is in (x, y) plane, LC material is filled in the middle cavity which is formed between the inverted circular patch and the ground plane. The bulk of LC material in the cavity can be treated as a substrate for characteristic analysis. Meanwhile, to control the direction of LC molecules, the patch and ground plane are also used as electrodes to provide bias voltage.

Several approaches have been adopted to design CPRs, including transmission line model, cavity model and full-wave simulations. In this work, cavity model and full-wave simulation were implemented to design the CPRs and characterize the LC materials used in the devices. Full-wave simulation is more accurate than any other models, however it needs a large number of optimization iterations and usually gives less physical insight. Whereas the cavity model is simpler and can indicate good physical insight. The following presents the main principle and key parameters of a cavity model. The results for a CPR design based on full-wave simulation and the cavity model are given

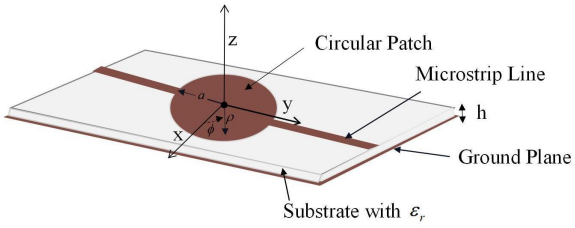

Figure 2. Geometry of a CPR with parameters of circular radius a, substrate height h and dielectric constant ε_r in a cylindrical coordinate (ρ, ϕ, z) system.

and compared in the end.

2.1. Cavity model of a CPR

RF properties of LC materials can be studied by using a CPR with the cavity model, which exploits the relationship between the resonant frequency and dielectric constant, and is a commonly-used method to estimate the permittivity ε_r and the loss tangent. As shown in Figure 2, since the substrate height h is much smaller than the wavelength of RF signal λ ($h << \lambda$), the primary electric and magnetic modes that are supported in a CPR are TM^z, where z is taken perpendicular to the patch.

Based on the electromagnetic field theory, the fields propagating in the cavity can be derived by using the vector potential method, which satisfies the homogeneous wave formulation in the cylindrical coordinate. In this section, the principle equations are provided to derive the dielectric properties, and more detailed description regarding the cavity model can be found in [29] and Appendix A. The resonant frequency corresponding to the permittivity for the dominant mode TM^z_{mn0} can be written as

$$f_{mn0} = \frac{1}{2\pi a\sqrt{\mu\varepsilon}}\left(\frac{\chi^{'}_{mn}}{a}\right) = \frac{\chi^{'}_{mn} v_0}{2\pi a\sqrt{\varepsilon_r}} \tag{2}$$

where f_{mn0} is the resonant frequency, which is the key parameter required to derive ε_r, and can be obtained from scattering parameters of S_{11} or S_{22} based on VNA measurements or the full-wave simulations. ε_r is the relative permittivity of LC material, a is the radius of the inverted circular patch, h is the height of LC in the cavity, v_0 is the speed of light in free space, $\chi^{'}_{mn}$ ($m = 0, 1, 2, \cdots, n = 1, 2, 3, \cdots$) is the zeros of the derivative of Bessel function $J_m(\chi)$ which is used to determine the order of resonant frequency. Therefore, according to a given TM^z_{mn0} mode, the dominant value of $\chi^{'}_{mn}$ can be calculated using the Bessel functions. Taking the first four modes of TM^z_{mn0} as an example, we can calculate, in ascending order, $\chi^{'}_{11} = 1.8412$, $\chi^{'}_{21} = 3.0542$, $\chi^{'}_{01} = 3.8318$, and $\chi^{'}_{31} = 4.2012$, respectively. Thus, by means of the known values of other parameters in (2), we can directly derive ε_r.

2.2. Effective radius of a circular patch

In practice, f_{mn0} predicted from the cavity model based on (2) is usually slightly higher than that from the measured results. The reason is that it does not take into account the fringing effect of the circular patch, which makes the electrical radius a

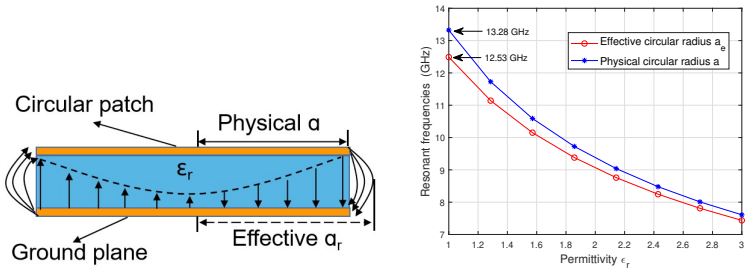

(a) Fringing effect of a circular patch.

(b) Resonant frequencies using the physical and effective circular radius, respectively.

Figure 3. Fringing effect and resonant frequencies corresponding to the circular radius a and effective radius a_e vs. different dielectric constants.

larger than the physical size, as shown in Figure 3a. To optimize the parameter for the cavity model and improve the estimate accuracy of ε_r, we need to compensate the extra length for the radius a. In this work, effective radius a_e is considered to include the fringing effect, and a good approximation is made in [32] and can be written as

$$a_e = a \times \left\{1 + \frac{2h}{\pi a \varepsilon_r}\left[\ln\left(\frac{\pi a}{2h}\right) + 1.7726\right]\right\}^{\left(\frac{1}{2}\right)}. \tag{3}$$

Based on the geometry of the proposed CPR ($a = 6.5\text{mm}, h = 0.265$ mm), when the range of the permittivity of $1 < \varepsilon < 3$ is considered, the resonant frequencies corresponding to the physical radius a and the effective radius a_e are calculated and plotted in Figure 3b, respectively. We can observe the frequencies determined from a_e by (3) are less than those with the physical radius a, which mainly because a_e is greater than a due to the the fringing effect. Meanwhile, the deviation decreases with an increase of ε_r and the maximum discrepancy is about 1 GHz when $\varepsilon_r = 1$. Adopting the effective radius a_e and taking $\chi_{11}^{'}$ as an example, the resonant frequency for the dominant mode TM_{110}^{z} of (2) can be rewritten as

$$f_{110} = \frac{\chi_{11}^{'} v_0}{2\pi a_e \sqrt{\varepsilon_r}} = \frac{1.8412 v_0}{2\pi a_e \sqrt{\varepsilon_r}}. \tag{4}$$

2.3. Determination of permittivity

With the known values of f_{110} and a_e, ε_r can be directly calculated using (4) and can be written as:

$$\varepsilon_r = \left(\frac{\chi_{11}^{'} v_0}{2\pi a_e f_{110}}\right)^2. \tag{5}$$

However, in order to calculate a_e using (3), we must know the value of ε_r, which means there is a high correlation between a_e and ε_r in (3), so we must decouple a_e from ε_r first. In the literature, considering the fact that $a >> h$ for LC-based devices (since h should be small enough to have a quick response time for tuning), and for the majority of microwave LC materials, ε_r is usually between 1.6 to 3.5 at sub-10 GHz

band. We can fit a_e by assuming different values to ε_r in the range from 1.6 to 3.5 in (3). With this approach, for the proposed CPR structure, the associated effective radius a_e with respect to a is obtained by interpolation method, and can be expressed as

$$a_e = \begin{cases} a + 0.04(\text{mm}), \varepsilon_r = 1 \\ a + 0.02(\text{mm}), 1.6 < \varepsilon_r < 3.5 \end{cases} \tag{6}$$

2.4. Determination of loss tangent

In addition to permittivity, loss tangent tanδ can be estimated by seeking the quality factor and the relationship between them is approximately given as [29]

$$\tan\delta \approx \frac{1}{Q} \tag{7}$$

where Q is the unloaded quality factor when the energy dissipation of conductor is considered and radiation loss is neglected in the microwave resonator. Accurate determination of loss tangent is a very complex task [30] since the loss from various sources is difficult to distinguish. For transmission type resonators such as a CPR, the loaded Q_L can be calculated as

$$Q_L = \frac{f_{mn0}}{f_1 - f_2} \tag{8}$$

where f_1 and f_2 are respectively the half-power frequencies according to the resonant frequency f_{mn0} for a given mode, which can be obtained at 3 dB power points deviated from the resonant frequency. The loss tangent tanδ is initially defined as [31]

$$\tan\delta = \frac{\varepsilon_r^{''}}{\varepsilon_r^{'}} \tag{9}$$

where $\varepsilon_r^{''}$ is the imaginary part of permittivity, which can be determined by

$$\varepsilon_r^{''} = \frac{V_c}{4V_s}(\frac{1}{Q_L} - \frac{1}{Q_0}) \tag{10}$$

where V_c is the volume of the empty cavity and Q_0 is the value of quality factor. When the LC is filled in the cavity, the value of the volume (V_s) remain unchanged. But the value of the quality factor will be reduced (Q_L). $\varepsilon_r^{'}$ is the real part of permittivity, which can be obtained as

$$\varepsilon_r^{'} = \frac{V_c(f_c - f_s)}{2V_s f_s} + 1 \tag{11}$$

where f_c is the resonant frequency with an empty cavity, and f_s is the resonant frequency after the NLC sample is filled. With (8), (9), (10) and (11), the loss tangent can be derived accordingly.

To sum up, according to the above-mentioned equations, ε_r and loss tangent tanδ can be determined by a full-wave simulation or VNA measurements. Taking the VNA

measurement as an example, f_{110} is obtained from the S-parameter (S_{11} or S_{22}) measurements with TM_{110} as the dominant mode, then we can derive the relative dielectric constant ε_r using (5) and the numerical approximation a_e defined in (6). Finally, loss tangent tanδ can be estimated by (9) with the corresponding frequencies.

2.5. Feasibility analysis of the cavity model

In order to verify the feasibility of the proposed cavity model, we first acquire the resonant frequencies using (4), then the results are compared with those from the full-wave simulation. The main parameters used for this analysis are identical to the fabricated CPR provided in Section 3, e.g., a=6.5 mm and h=0.265 mm. Five distinct dielectric constants are assigned separately (the range from 2.22 to 2.98) for verification, we obtained the resonant frequencies based on the cavity model and the full-wave simulation, respectively, as illustrated in Figure 4. In Figure 4, the curves represent the refection coefficient S_{11} from the full-wave simulation, and the straight lines are the frequencies calculated by using (4) from the cavity model. Taking $\varepsilon_r = 2.22$ as an example, the resonant frequency from the lowest value of S_{11} using the full-wave simulation is 8.84 GHz, and it is estimated 8.81 GHz based on the cavity model, the discrepancy is only 0.03 GHz, which is close enough to demonstrate the high accuracy on determination of dielectric characteristics through the cavity model.

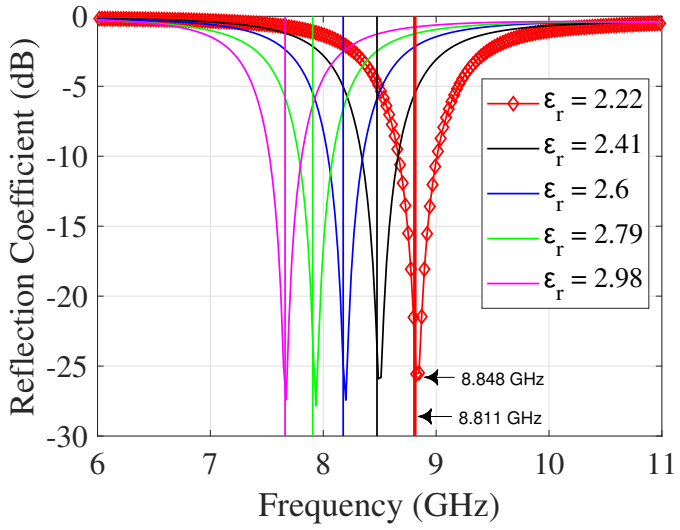

Figure 4. Comparison of the resonant frequencies from the cavity model and a full-wave simulation vs. different values for dielectric constant of the LC material.

3. Experimental results and discussion

To accurately evaluate the characteristics of LC in mmW band, a CPR was designed with the optimized parameters by a full-wave simulation. Three prototypes were fabricated and tested. The experimental results including permittivity and loss tangent for the two types of newly-developed LC materials are provided and verified.

3.1. Design and fabrication

Figure 5 illustrates the structure of the proposed CPR, LC is contained in a closed cavity between the circular patch on the top and the ground plane on the bottom. As shown in Figure 5 (a), on top layer three holes are designed for filling the LC material, the diameter of each hole is 1 mm. A cavity for LC cell is produced on middle layer, the ground plane is fabricated with a 40 mm × 24 mm × 1 mm copper sheet. The top layer and middle layer have the same thickness of 0.254 mm, and are made of commercially available FM4BX with different dielectric permittivity where $\varepsilon_r = 2.2$ for the former and $\varepsilon_r = 3$ for the latter. The geometry of other parameters are given in Figure 5 (b).

In contrast to a conventional CPR design, this work proposed a coupling mechanism for microwave transmission, to avoid the possible damage to the instrument caused by a higher bias voltage. Instead of a direct contact through the vias, we used copper patches to couple the RF signal between the transmission line of the resonator and the CPWs for feeding, as shown in 5 (c). More detailed analysis on the coupling mechanism is given in Subsection 3.2.

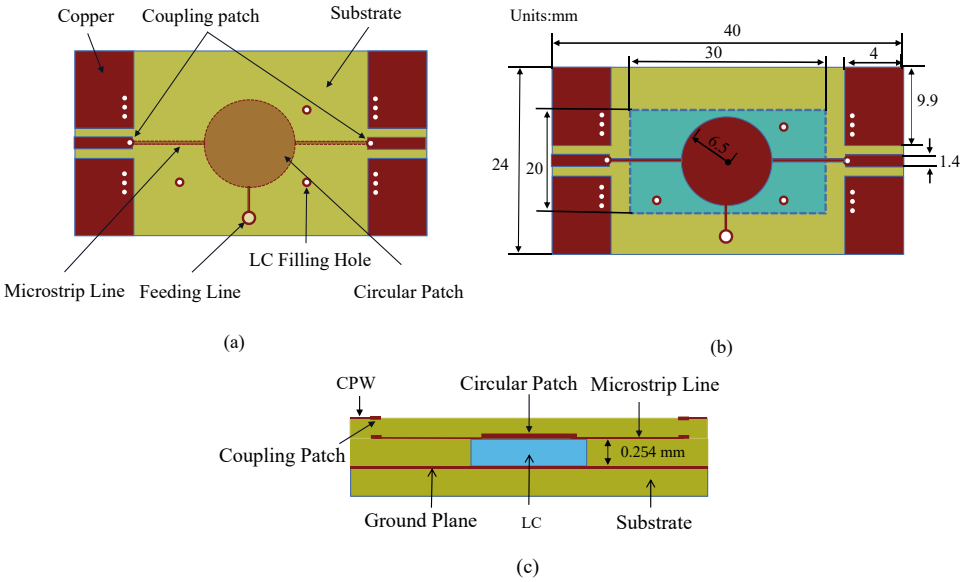

Figure 5. Structure of the proposed CPR device. **(a)** Top view of the first layer. **(b)** Dimensions of the CPR. **(c)** Side view of the CPR with three layers.

Figure 6 shows the key fabrication processes of the CPR. The top board consists of the primary elements, including an inverted circular patch, coupling patches, CPWs, feeding lines, and filling holes, CPWs are designed with a 50-Ω characteristic impedance, as shown in Figure 6 (a). The board after the deposition and curing treatments with Polyimide (PI, AL 1254) on the patch surface is presented in Figure 6 (b), the thickness of PI is about 100 nm and the curing process at 230 °C took 20 minutes. The microscopic grooves are realized by rubbing the PI surface with velvet in the same direction, shown in Figure 6 (c). Figure 6 (d) illustrates the device under test (DUT) by a vector network analyzer (VNA, N9918A of Keysight).

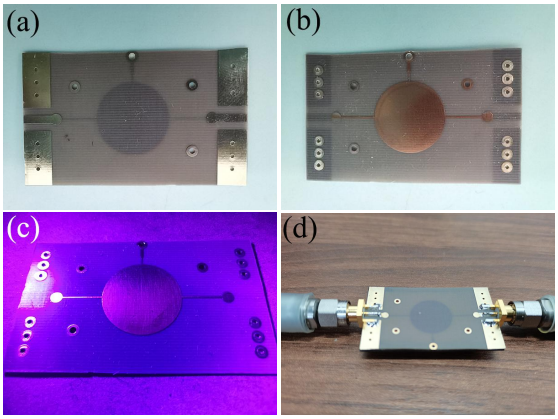

Figure 6. Key fabrication steps for the CPR: (**a**) main board including the circular patch, (**b**) depositing and curing treatment of PI on the patch surface, (**c**) microscopic grooves on the PI surface, and (**d**) a CPR under test using a VNA.

Table 1. Resonant frequency and calculated permittivity for air from the CPR with the coupling mechanism and vias connection (where $\varepsilon_r = 1$ is the norm).

Parameter	**Frequency (GHz)**	**Permittivity (ε_r)**
Experiment(coupling)	12.48	1.0→0.994
Full-wave simulation(coupling)	12.45	1.0
Full-wave simulation(vias)	12.33	1.0→1.06

3.2. Experiments

In this section, experiments are carried out to estimate the dielectric characteristics of new developed LC materials. The procedure to determine the dielectric properties of the NLCs are summarized into three steps: Step 1, the reflection coefficients of DUTs are acquired by using the VNA, to determine the resonant frequencies. Step 2, the values of dielectric constant ε_r are calculated using (5) by the cavity model. Finally, ε_r obtained from Step 2 was further verified with the full-wave simulation.

As mentioned earlier, in order to support higher bias voltages for achieving the full anisotropy potential, a coupling mechanism is proposed for feeding the resonator in this work. Thus we first analyze the impact of the coupling mechanism, in comparison to conventional vias arrangements. The relativity permittivity of air (where $\varepsilon_r = 1$ without the presence of the LC material) is used as a testing benchmark to evaluate the accuracy of the method. The scattering parameter S_{11} obtained from measurement and the full-wave simulation is shown in Figure 7. It depicted that the coupling mechanism pushes the resonant frequency slightly towards higher frequency compared with via arrangement. When the coupling mechanism is employed, we observe that the resonant frequency from measurement (12.48 GHz) is very close to that from simulation (12.45 GHz) (see Table 1 for details).

Two types of LC mixtures, JC-M-LC-E7 from JCOPTIX and QYPD-470-10-N001 from Qingdao QY Liquid Crystal Co., are used for testing. They are commercially available and both have been developed primarily for optical applications. Their dielectric properties at the optical spectrum are summarized in Table 2 but short of description on characteristics at microwave frequencies, and the molecule structure of the intermediate compounds for typical E7 mixtures is depicted in Figure 8. They can be potentially employed to design and manufacture microwave or mmWave compo-

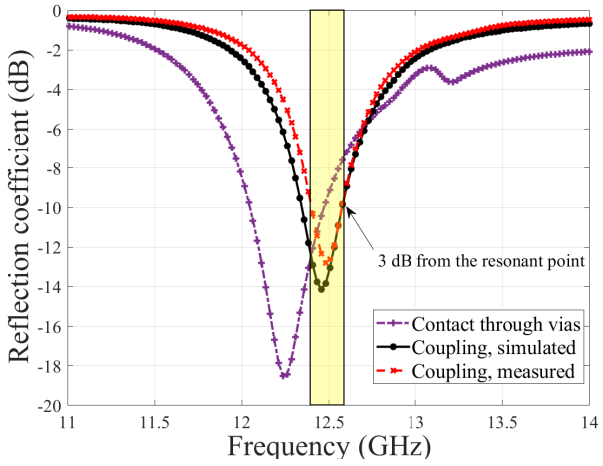

Figure 7. Scattering parameters of the empty CPR device with the coupling mechanism and via connection without LC filled in the cavity ($\varepsilon_r = 1$).

Table 2. Comparison of dielectric properties of available new NLCs and classical mixture E7 (Merck) for display applications.

LC	n_e	n_o	Δn @589 nm	$\epsilon_{r,\perp}$	$\epsilon_{r,\parallel}$	$\Delta\epsilon_r$ @1 KHz	Clearing point T_c (°C)
E7(Merck)	1.739	1.523	0.216	5.2	19.6	14.4	58
QYPD-470-10-N001	1.778	1.523	0.275	6.5	20	13.5	101
JC-M-LC-E7	1.741	1.517	0.224	5.3	16.7	11.4	58

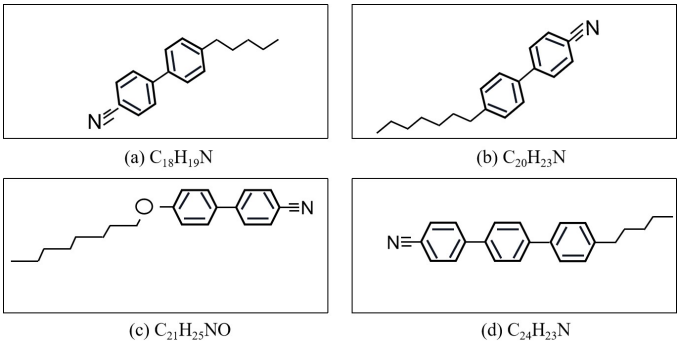

Figure 8. Molecule structures for typical E7 intermediate compounds, and associated empirical formulas.

nents. Thus this study investigates their dielectric characteristics (dielectric constant and loss tangent) at the microwave frequency bands. It is pointed out that for JC-M-LC-E7, this is the first time to examine its properties in microwave frequencies as far as we understand.

To determine the anisotropy and loss tangent of the two types of LCs (JC-M-LC-E7 and QYPD-470-10-N001), the experiments were performed by applying external bias voltages. To reduce the random errors, three devices dubbed as DUT1, DUT2, and DUT3, were fabricated, as shown in Figure 9. The LC material was filled into the cavity through the filling holes, and a 1 KHz sine wave voltage is applied with a AC power source. By adjusting the voltage step by step, a largest phase shift was observed when the bias voltage was reaching 32 V (the peak to peak voltage), where the long

axis of the LC molecules was expected to be approximately in parallel to electric field of the propagated waves.

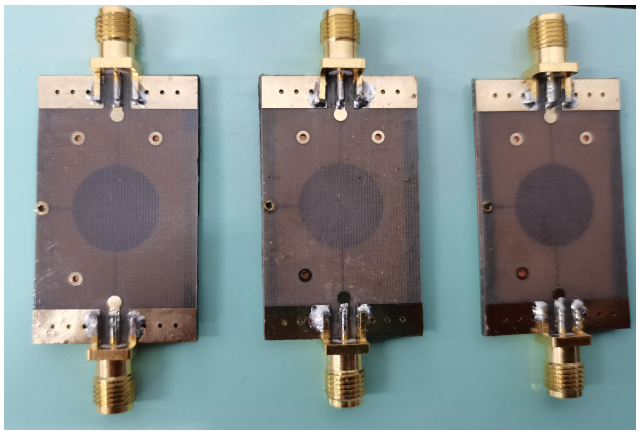

Figure 9. Three CPR devices manufactured for material characterization.

When JC-M-LC-E7 was filled in the cavity of DUT1, Figure 10 demonstrates the scattering parameter S_{11} obtained from the VNA and full-wave simulation, respectively. We can see there is a good agreement on the resonant frequency between simulation and experiments, whether 0 or 32 V voltage was applied. In Figure 11, S_{11} for JM-M-LC-E7 from experiments using three DUTs was presented. As expected, three DUTs have the approximate performance. The similar results for QYPD-470-10-N001 were also observed, as shown in Figure 12. Using the frequencies acquired from measurements, the dielectric constant and loss tangent for both types of LC mixtures were calculated based on the cavity model, and the results were listed in Table 3 and Table 4, respectively. The term unbiased and biased in these tables mean that 0 and 32 Volts are applied, respectively.

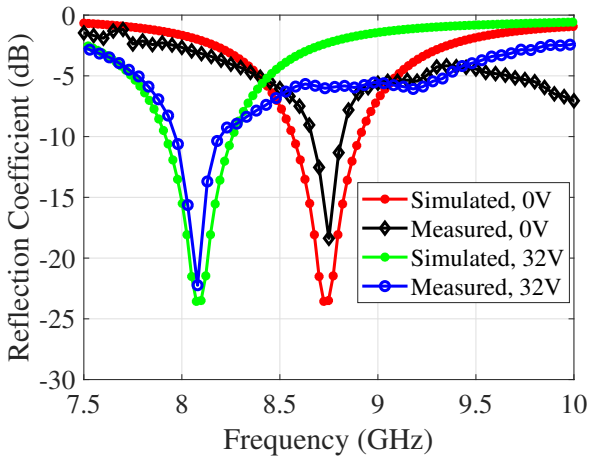

Figure 10. Scattering parameter S_{11} for JC-M-LC-E7 from the full-wave simulation and experiment using DUT1 at 0 and 32 V, respectively.

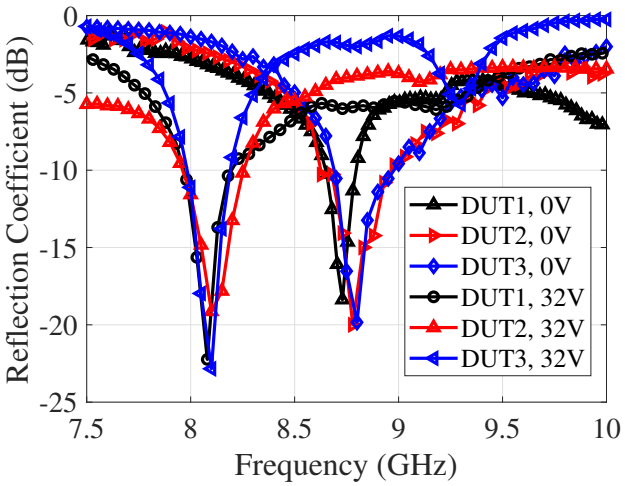

Figure 11. Scattering parameter S_{11} for JC-M-LC-E7 from experiments using three DUTs at 0 and 32 V, respectively.

Table 3. Resonant frequency, calculated dielectric constant and loss tangent for JC-M-LC-E7 using three DUTs.

Device	Condition	Resonant frequency (GHz)	tanδ	Permittivity
DUT 1	unbiased	8.73	0.045	2.27
	biased	8.07	0.018	2.70
DUT 2	unbiased	8.78	0.042	2.24
	biased	8.12	0.016	2.65
DUT 3	unbiased	8.80	0.041	2.23
	biased	8.14	0.014	2.63

3.3. Uncertainty analysis

Uncertainty may exist in every step of the investigation. There were many potential sources of errors, such as material stability, manufacturing tolerance, optimal position for biasing, etc. Two key steps have been taken to reduce the uncertainty:

1) Coupling mechanism is used to make connection between the transmission line where the CPR is connected to and the CPW, which can obtain a more stable and accurate measurement than the case where a direct connection exists through a vias, especially for higher external voltages.

2) More than one samples have been made for cross checking and reducing the uncertainty. Three devices have been fabricated to make reliable test for the proposed method. The resonant frequencies and the corresponding dielectric constant from the measurement and simulation are summarized in Table 5, and a slight discrepancy

Table 4. Resonant frequency, calculated dielectric constant and loss tangent for QYPD-470-10-N001.

Device	Condition	Resonant frequency (GHz)	tanδ	Permittivity
DUT 1	unbiased	8.61	0.072	2.33
	biased	7.59	0.009	3.04
DUT 2	unbiased	8.66	0.071	2.29
	biased	7.53	0.007	3.08
DUT 3	unbiased	8.71	0.070	2.28
	biased	7.56	0.007	3.06

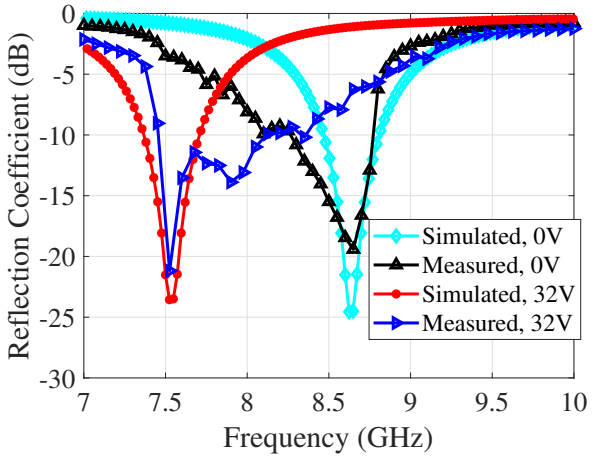

Figure 12. Scattering parameter S_{11} for QYPD-470-10-N001 from the full-wave simulation and experiment using DUT1 at 0 and 32 V, respectively.

Table 5. Uncertainty analysis based on resonant frequency and interpolation from full-wave simulations when the cavity is empty.

Devices	**Resonant freq. (GHz)**	Δf**, Freq. dev. (GHz)**	$\hat{\epsilon}_r$	$\Delta\epsilon_r$
Simulated	12.45	0.00	1.00	0.0
DUT 1	12.48	+0.03	0.994	-0.006
DUT 2	12.53	+0.08	0.985	-0.015
DUT 3	12.56	+0.11	0.980	-0.020

among these devices is observed. It is shown that the error for anisotropy determination is within a scope of 0.02.

To clearly demonstrate the performance of the proposed CPR, uncertainty comparison between the proposed method and other similar methods in the literature is listed in Table 6. As shown in Table 6, the uncertainty for the permittivity determination proposed by this work is about 0.02, which is much lower than that based on other conventional techniques, a significant improvement is observed.

3.4. Discussion

This work shows that the resonator based technique can achieve a high accuracy in determining permittivity and loss tangent of NLC with a low cost. However, there are still some problems to be addressed in the future work. For example, although we have made some analysis on the effect of coupling mechanism, quantitative analysis such as numerical model, propagation characteristics and impedance mismatching, should be

Table 6. Uncertainty comparison of the proposed work to that of methods found in the literature.

Method	**Freq. (GHz)**	$\epsilon_{r\perp}$	$\epsilon_{r\parallel}$	$\Delta\epsilon$	**Uncertainty**
Split-Cylinder Ring [24]	5	2.28	3.08	0.8	$\pm$0.22
Patch Resonator [26]	40	2.74	3.16	0.42	0.1
Circular Patch Resonator [27]	4.8-8.7	2.69	3.12	0.43	0.07
This work (JC-M-LC-E7)	5-10	2.25	2.67	0.42	0.02

investigated more thoroughly.

The alignment procedure is critical to establish and control the relationship between the orientation of the LC molecules and polarization of the waves propagating through the material. However, we can not evaluate the performance of alignment procedure by some simple methods. In addition, one of the concerns in practical applications is the response time of LC. which depends primarily on the thickness of the LC cells. The response time is not the main focus of this study and would be investigated in future studies.

4. Conclusions

A technique using a CPR to determine the dielectric constant and loss tangent of NLC materials has been developed and validated at a moderately low cost. Numerical methods, including the cavity model and the full-wave simulation, are used to assess the CPR performance with the optimized design parameters, aiming for a high-level determination accuracy for material characterisation. Three prototypes are manufactured with a PCB-based process and measured to reduce the random errors. The results demonstrate a good agreement between the simulation and experimental measurements. The uncertainty for determining anisotropy of the NLC materials based on the proposed CPR is below 0.02, which is significantly lower than that reported in the literature. The proposed method can be used to design high-performance microwave devices at microwave and mmWave frequency bands.

Acknowledgement(s)

The authors would like to thank Miss Huijuan Xing for her help in fabrication of the prototypes in this study.

Disclosure statement

No potential conflict of interest was reported by the authors.

ORCID

Yongwei Zhang, https://orcid.org/0000-0001-9201-4511

Funding

This work was supported in part by the Basic Science Research Program of Nantong City JC2020142, in part by the NSFC under Grants 62174091 and 62201294, in part by Post-Doc International Exchange Programme YJ20210098.

References

[1] Jakoby R, Gaebler A, Weickhmann C. Microwave liquid crystal enabling technology for electronically steerable antennas in satcom and 5G millimeter-wave systems. Crystals. 2020;10(6):514.

[2] Li JF. Challenges and opportunities for nematic liquid crystals in radio frequency and beyond. Crystals. 2022;12(5):632.

[3] Yang JG, Yang K. Ka-band 5-bit MMIC phase shifter using InGaAs PIN switching diodes. IEEE Microw Wireless Compon Lett. 2011;21(3):151-153.

[4] Kim HT, Park JH, Lee S, et al. V-band 2-b and 4-b low-loss and low-voltage distributed MEMS digital phase shifter using metal-air-metal capacitors. IEEE Trans Microw Theory Tech. 2002;50(12):2918-2923.

[5] Nafe A, Shamim A. An integrable SIW phase shifter in a partially magnetized ferrite LTCC package. IEEE Trans Microw Theory Tech. 2015;63(7):2264-2274.

[6] Li JF, Chu DP. Liquid crystal-based enclosed coplanar waveguide phase shifter for 54–66 GHz applications. Crystals. 2019;9(12):650.

[7] Zou J, Yang Q, Hsiang EL, et al. Fast-response liquid crystal for spatial light modulator and LiDAR applications. Crystals. 2021;11(2):93.

[8] Wolinski TR, Czapla A, Ertman S, et al. Photonic liquid crystal fibers for sensing applications. IEEE Trans Instrum Meas. 2008;57(8):1796-1802.

[9] Polat E, Tesmer H, Reese R, et al. Reconfigurable millimeter-wave components based on liquid crystal technology for smart applications. Crystals. 2020;10(5):1-39.

[10] Wang SH, Li Z, Chen XX, et al. A liquid crystal leaky-wave antenna with fixed-frequency beam scanning and open-stop-band suppression. Liq Cryst. 2022;49(11):1403-1410.

[11] Tesmer H, Razzouk R, Polat E, et al. Temperature characterization of liquid crystal dielectric image line phase shifter for millimeter-wave applications. Crystals. 2021;11(1):63.

[12] Sun SY. Electronically tunable liquid-crystal-based F-band phase shifter. IEEE Access. 2020;8:151065-151071.

[13] Yang J, Cai C, Yin Z, et al. Reflective liquid crystal terahertz phase shifter with tuning range of over 360 degrees. IET Microw Antenna Propag. 2018;12(9):1466-1469.

[14] Li X, Wan Y, Liu J, et al. Broadband electronically scanned reflectarray antenna with liquid crystals. IEEE Antennas Wireless Propag Lett. 2021;20(3):396-406.

[15] Tesmer H, Gold G, Bachbauer F, et al. Feasibility of additively manufactured tunable liquid crystal loaded dielectric waveguides. IEEE Microw Wireless Compon Lett. 2021; 31(8):973-976.

[16] Lang TN, Bui VB, Inoue Y, et al. Response improvement of liquid crystal-loaded NRD waveguide type terahertz variable phase shifter. Crystals. 2020;10(4):307.

[17] Polat E, Reese R, Tesmer H, et al. Fully dielectric phased array for beamsteering using liquid crystal technology at w-band. Proceedings of the 2020 14th European Conference on Antennas and Propagation (EuCAP); 2020 March 15–20; Copenhagen, Denmark.

[18] Karabey OH, Gaebler A, Strunck S, et al. A 2-D electronically steered phased-array antenna with 2×2 elements in LC display technology. IEEE Trans Microw Theory Tech. 2012;6(5):1297-1306.

[19] Jost M. Liquid crystal mixed beam-switching and beam-steering network in hybrid metallic and dielectric waveguide technology[dissertation]. Darmstadt: TU Darmstadt at Darmstadt; 2018.

[20] Carr EF, Spence RD. Influence of a magnetic field on the microwave dielectric constant of a liquid crystal. J Chem Phys. 1954;22(9):1481-1486.

[21] Mueller S, Penirschke A, Damm C, et al. Broad-band microwave characterization of liquid crystals using a temperature-controlled coaxial transmission line. IEEE Trans Microw Theory Tech. 2005;53(6):1937-1945.

[22] Bulja S, Mirshekar D, James R, et al. Measurement of dielectric properties of nematic liquid crystals at millimeter wavelength. IEEE Trans Microw Theory Tech. 2010;58(12):3493-3501.

[23] Peng HF, Zhang YW, Zhu SL, et al. Determining dielectric properties of nematic liquid crystals at microwave frequencies using inverted microstrip lines. Liq Cryst. 2022;49(15):2069-2081.
[24] Sánchez JR, Nova V, Bachiller C, et al. Characterization of nematic liquid crystal at microwave frequencies using split-cylinder resonator method. IEEE Trans Microw Theory Tech. 2019;67(7):2812-2820.
[25] Gao C, Li E, Zhang Y, et al. Permittivity measurement of the dielectric material at the off-axis position in a cylindrical cavity. IEEE Trans Microw Theory Tech. 2021;69(3):1711-1722.
[26] Yazdanpanahi M, Bulja S, Mirshekar-Syahkal D, et al. Measurement of dielectric constants of nematic liquid crystals at mm-wave frequencies using patch resonator. IEEE Trans Instrum Meas. 2010;59(12):3079-3085.
[27] Schaub DE, Oliver DR. A circular patch resonator for the measurement of microwave permittivity of nematic liquid crystal. IEEE Trans Microw Theory Tech. 2011;59(7):1855-1862.
[28] Utsumi Y, Kamei T. Dielectric permittivity of liquid crystal in the microwave and millimetre range. Mol Cryst Liq Cryst. 2004;409(1):355–370.
[29] Balanis CA. Antenna theory analysis and design. 4th ed. New Jersey(NJ): John Wiley & Sons; 2016.
[30] Chen LF, Ong CK, Neo CP. Microwave electronics: measurement and materials characterization. New York(NY): John Wiley & Sons; 2004.
[31] Czichos H, Saito T, Smith L. Measurement of materials dielectric properties. In: Czichos H, Saito T, Smith L, editors. Springer Handbook of Material Measurement Method. New York(NY): Springer; 2006. p. 472-481.
[32] Shen L, Long S, Allerding M, et al. Resonant frequency of a circular disc, printed-circuit antenna. IEEE Trans Antennas Propag. 1977;25(4):595-596.
[33] Eremenko ZE, Shubnyi AI, Kogut AY, et al. High loss liquid dielectric characterization: Comparison of microwave waveguide and resonator measurement techniques. Int J Microwave and Wireless Tech. 2020;12(9):892-899.
[34] Nobles JE, Melnyk O, Glushchenko A, et al. Effect of alignment methods on liquid crystal performance in millimeter wave devices. Engineering Research Express. 2020;2(2):025002.

Appendix A. Mathematical expressions for calculating the resonant frequencies of a CPR

Applying the magnetic vector potential theorem, the potential A_z satisfies the Helmholtz wave equation,

$$\nabla A_z(\rho, \phi, z) + k^2 A_z(\rho, \phi, z) = 0 \tag{A1}$$

where A_z is the magnetic vector potential, ∇ is the Laplace operator. For TM^z models, the electromagnetic fields can be written as

$$\begin{cases} E_\rho = -j\dfrac{1}{\omega\mu\varepsilon}\dfrac{\partial^2 A_z}{\partial\rho\partial z} \\ H_\rho = \dfrac{1}{\mu}\dfrac{1}{\rho}\dfrac{\partial A_z}{\partial\phi} \\ E_\phi = -j\dfrac{1}{\omega\mu\varepsilon}\dfrac{1}{\rho}\dfrac{\partial^2 A_z}{\partial\phi\partial z} \\ H_\phi = -\dfrac{1}{\mu}\dfrac{\partial A_z}{\partial\rho} \\ E_z = -j\dfrac{1}{\omega\mu\varepsilon}\left(\dfrac{\partial^2}{\partial z^2}+k^2\right)A_z \\ H_z = 0 \end{cases} \tag{A2}$$

subject to the boundary conditions

$$\begin{cases} E_\rho(0\le\rho\le a, 0\le\phi\le 2\pi, z=0)=0 \\ E_\rho(0\le\rho\le a, 0\le\phi\le 2\pi, z=h)=0 \\ H_\phi(\rho=a, 0\le\phi\le 2\pi, 0\le z\le h)=0. \end{cases} \tag{A3}$$

A_z can be derived as

$$A_z = B_{mnp}J_m(k_\rho\rho)[A_2\cos(m\phi)+B_2\sin(m\phi)]\cos(k_z z) \tag{A4}$$

with the constraint equation

$$(k_\rho)^2+(k_z)^2 = k_r^2 = \omega_r^2\mu\varepsilon. \tag{A5}$$

where k_ρ and k_z can be calculated as

$$\begin{aligned} &k_\rho = \frac{\chi'_{mn}}{a} \\ &k_z = \frac{p\pi}{h} \\ &m = 0,1,2,3\cdots \\ &n = 1,2,3,\cdots \\ &p = 0,1,2,3,\cdots. \end{aligned} \tag{A6}$$

Appendix B. Author details

Qiang Wu received the M.S. degree in School of Information Science and Technology from Southwest Jiaotong University, Chengdu, China, in 2006, and the Ph.D. degree in the School of Electronic Information at Wuhan University, Wuhan, in 2019. He is currently an associate professor with the School of Transportation, Nantong

University, China. His research interests include antenna array design and satellite navigation techniques.

Yongwei Zhang (M'07) received the B.S. degree in Communication Engineering from Jilin University in 1996, and the Ph.D. degree from School of Electrical and Electronic Engineering, The University of Manchester, U.K., in 2007. In 1996, he joined Lucent Technologies (AT&T initially), China, where he was an application engineer on 5ESS® system, and later a system engineer and had been worked for Lucent until 2003. While he was working for Lucent, in 1998, he was sent as a visitor to the Bell Laboratories, Indian Hill, Naperville, IL, USA, trained in communication system engineering tool development and later certified as an international instructor. In the years working for Lucent Technologies from 1996 to 2003, he had been involved in 5ESS® Switch application engineering and optimization for wireless communication systems. In 2003, he joined The University of Manchester first as a Ph.D. student and later a Research Fellow, then the task leader of the front-end design work package in Mid-Frequency Aperture Array Consortium for the Square Kilometre Array (SKA). His current research interests include antenna and array designs based on flexible material, electromagnetic theories, antenna array calibration techniques, and radio astronomy instrumentation.

Haofeng Peng was born in Ningde, Fujian Province, China, in 1998. He received the B.S. degree in Communication Engineering from Putian University, Putian, China, in 2021. He is currently working towards the M.S. degree at Nantong University. His current interests include antenna array design, microwave devices based on nematic liquid crystal.

Murat Temiz (M'20) received the B.S. degree from Gazi University, Ankara, Turkey, in 2011, and the M.S. degree from the TOBB University of Economics and Technology, Ankara, in 2013. Then he joined the Department of Electrical and Electronic Engineering, The University of Manchester, Manchester, U.K. for his Ph.D. degree, at the same time also working as a Research Assistant focusing on massive multiple-input–multiple-output (MIMO) communication, MIMO orthogonal frequency-division multiplexing (OFDM) radars, and energy efficiency, he obtained his Ph.D. degree in 2020. His current research interests include massive MIMO systems, antenna array design, channel measurements, optimization, dual-functional MIMO OFDM radar communication systems, and machine learning applications.